

Cardio-Respiratory Motion Decomposition for Myocardial Motion Modelling in TECAB

Osemwaro Pedro, Daniel Rueckert, and Philip J. Edwards

Department of Computing, Imperial College London
{op02,dr,eedwards}@doc.ic.ac.uk *

Abstract. In this paper we propose a framework for the analysis of the cardiac and respiratory motion of the myocardium based on stereo video images taken from a surgical robot. Our aim is to use the analysis results as the basis for a myocardial surface reconstruction algorithm. These results will provide important prior information that will be needed to obtain accurate surface point matching in homogeneous regions and in areas of high deformation.

We show how to fit a parametric cardio-respiratory model to myocardial surface features, and we present methods for validating the model.

1 Introduction

There have been a number of recent technological advances in cardiac surgery aimed at making the procedures less invasive. These include minimally-invasive direct coronary artery bypass (MIDCAB) and totally endoscopic coronary artery bypass (TECAB). In TECAB, the entire procedure is performed robotically through small incisions on the beating heart, without the need for a cardiopulmonary bypass.

However, TECAB procedures still suffer from a relatively high rate of conversion to either MIDCAB or conventional open-chest surgery [1–3]. Reasons for this include difficulty in locating an artery or vessel misidentification. Augmented reality (AR) guidance has the potential to reduce the conversion rate by overlaying an accurately registered graphical representation of a preoperative imaging model onto the surgeon’s view of the patient.

The da VinciTM robot provides an ideal device for such guidance due to the high quality 3D visualisation it provides. Previous researchers have demonstrated AR on phantom or animal data [4–6] or visualisation of intraoperative ultrasound [7]. Our aim is to augment the da VinciTM robot’s display with a 4D model of the beating heart preoperatively constructed from clinical data.

In order to register a preoperative 4D model to the robot’s intraoperative, stereo video images, it is necessary to reconstruct the 4D myocardial surface from the stereo video images. In [8], Stoyanov presents a method for sparse myocardial surface reconstruction based on tracking features in 3D, and in [9] he describes a method for dense reconstruction based on piecewise bilinear maps. Neither

* We are thankful to the EPSRC, grant EP/C523008/1.

of these methods take into account prior information about myocardial motion however (apart from assuming smoothness). Such information could potentially be used to improve point matching in areas of high deformation, and to infer more accurate interpolation methods for reconstructing the large homogeneous regions in which point matching fails.

The value of exploiting the periodicity of myocardial motion is shown by Ortmaier in [10], where the trajectory of an occluded feature is accurately predicted based on its past motion and the motion of other visible features, with which its motion is correlated. Accurate predictions such as this can be incorporated into a motion model to provide strong prior information for feature tracking.

In this paper we will focus on measuring the myocardial motion and decomposing it into cardiac and respiratory components. Knowing how much cardiac and respiratory motion is likely to occur between two consecutive video frames provides us with prior information that allows us to put empirically-supported bounds on the state space that a feature tracking algorithm must search. In order to achieve accurate sparse 4D reconstruction (which will be the initial stage of our dense reconstruction), a tracking algorithm must make effective use of such prior information.

2 Method

Our experiment is based on the trajectories of myocardial features manually tracked in stereo intraoperative videos of a patient. The trajectories were reconstructed in 3D after calibrating the cameras. Before we could measure the cardiac and respiratory components of the motion of the features, we had to decompose the trajectories into these components. We based our decomposition on the following assumptions:

- The motion of each feature is the sum of cardiac motion, respiratory motion and some amount of noise (noise being a result of tracking errors and random fluctuations in the cardio-respiratory motion).
- The cardiac and respiratory motions are periodic up to the effects of noise¹.

2.1 Motion Decomposition

In [11] a Cardiac Respiratory Parametric Model (CRPM) is used to describe the motion of the coronary arteries extracted from angiographic images. We have adopted this model to characterize the motion patterns of myocardial surface features. The CRPM models the motion of a myocardial feature as the sum of two periodic B-splines with uniform knot vectors, parameterised by the cardiac phase and the respiratory phase.

¹ The patients are under general anaesthetic during the operation, so variations in cardiac motion should be small. It is also reasonable to assume that variations in the respiratory motion are small, as the patient's breathing is mechanically controlled by a respirator.

So, suppose the trajectory of feature f in an arbitrary dimension is given by: $\mathbf{x}_f = (x_{f,0}(\chi_0, \rho_0), \dots, x_{f,T-1}(\chi_{T-1}, \rho_{T-1}))^T$, where $\chi_t \in [0, 1]$ and $\rho_t \in [0, 1]$ are measures of the cardiac and respiratory phases at time t . The CRPM approximates each $x_{f,t}(\chi_t, \rho_t)$ as $\hat{x}_{f,t}(\mathbf{v}, \chi_t, \rho_t)$, defined as follows:

$$\hat{x}_{f,t}(\mathbf{v}, \chi_t, \rho_t) \equiv \sum_{i=0}^{n_\chi - p_\chi - 1} b_{i,p_\chi}^C(\chi_t) v_i + \sum_{i=0}^{p_\chi - 1} b_{n_\chi - p_\chi + i, p_\chi}^C(\chi_t) v_i + \sum_{i=0}^{n_\rho - p_\rho - 1} b_{i,p_\rho}^R(\rho_t) v_{n_\chi + i} + \sum_{i=0}^{p_\rho - 1} b_{n_\rho - p_\rho + i, p_\rho}^R(\rho_t) v_{n_\chi + i} \quad , \quad (1)$$

where: p_χ/p_ρ are the degrees of the cardiac/respiratory B-splines; n_χ/n_ρ are the numbers of cardiac/respiratory B-spline control points; $\mathbf{v} \equiv (v_0, \dots, v_{n_\chi - p_\chi - 1}, v_{n_\chi}, \dots, v_{n_\chi + n_\rho - p_\rho - 1})^T$ is a vector of the first $n_\chi - p_\chi$ cardiac B-spline control points followed by the first $n_\rho - p_\rho$ respiratory control points (the last p_χ/p_ρ control points of the cardiac/respiratory B-splines are a repetition of the first p_χ/p_ρ . This makes the B-splines periodic); $b_{i,d}^C$ and $b_{i,d}^R$ are the degree d basis functions at control point i for the knot vectors associated with the cardiac and respiratory B-splines respectively.

We want to find the control points that minimise the squared error between the estimate and the true feature trajectory:

$$\mathbf{v} = \arg \min_{\mathbf{v}'} \|\mathbf{x}_f - (\hat{x}_{f,0}(\mathbf{v}', \chi_0, \rho_0), \dots, \hat{x}_{f,T-1}(\mathbf{v}', \chi_{T-1}, \rho_{T-1}))^T\|^2 \quad , \quad (2)$$

The linear least squares solution to (2) is given by the product of the pseudoinverse of a matrix B of the blending coefficients and \mathbf{x}_f . We used a Tikhonov regularisation matrix S of second-order central difference coefficients to minimise the curvature of the respiratory component to a degree controlled by α .

$$\mathbf{v} = (B^T B + \alpha^2 S^T S)^{-1} B^T \mathbf{x}_f \quad , \quad (3)$$

The reader is referred to [11] for a more detailed description of the terms of this solution.

2.2 Parameter Estimation by k -Fold Cross Validation

As in [11], we used cubic B-splines ($p_\chi = p_\rho = 3$). We used k -fold cross validation to find values for n_χ , n_ρ and α in a finite search space that would: (i) minimise the model's error over test data that was omitted from the model fitting procedure; and (ii) minimise the Cardiac Cycle Registration (CCR) error (see next section) over the test data.

Given values for n_χ , n_ρ and α , we calculated the average prediction error $e(n_\chi, n_\rho, \alpha)$ as follows:

- Partition the trajectory \mathbf{x}_f into k equal parts, omit part i and calculate (3) with the remaining $k - 1$ parts.

- Evaluate the RMS error $\sqrt{E_i[\epsilon^2]}$ between the model and the omitted part, and the CCR error ϵ_i^{CCR} over the omitted part.
- $e(n_\chi, n_\rho, \alpha) \equiv \frac{\sum_i (\sqrt{E_i[\epsilon^2]} + \epsilon_i^{\text{CCR}})}{k}$, the sum of the RMS model fitting errors and the CCR errors, averaged over the k parts.

Large values of k are preferable, as they allow $e(n_\chi, n_\rho, \alpha)$ to be calculated over more test data sets. However the value of k chosen should be small enough for each partition to contain at least one respiratory cycle.

2.3 Cardiac Cycle Registration

No motion decomposition validation was given in [11]. However under the periodicity assumptions stated above, subtracting the respiratory component of the CRPM from the data should leave us with the periodic cardiac motion and a small amount of noise. Hence, after subtracting the respiratory component and temporally registering the cardiac cycles of the resultant data to each other, we should be left with a set of cardiac trajectories that are accurately registered both temporally *and* spatially. The spatial variance in the temporally-registered trajectories thus gives us a measure of the accuracy of the CRPM’s respiratory motion estimation.

To make this more concrete, suppose the CRPM is parameterised with control point vector \mathbf{v} . We remove the model’s respiratory component from the data with $x'_{f,i} = x_{f,i}(\chi_i, \rho_i) - \hat{x}_{f,i}(\mathbf{v}, 0, \rho_i)$. We then draw m samples at corresponding phases from each cardiac cycle of \mathbf{x}'_f (uniformly-spaced in their phases). Let these samples form an $m \times c$ matrix X , where: $X_{i,j}$ is the i^{th} sample of the j^{th} cycle and c is the number of cardiac cycles in \mathbf{x}'_f . The CCR error ϵ^{CCR} is taken as the standard deviation of samples drawn from a given cardiac phase, averaged over all sampled phases, i.e.:

$$\epsilon^{\text{CCR}} = \frac{1}{m} \sum_i \left[\sqrt{\frac{1}{c} \sum_j X_{i,j}^2 - \left[\frac{1}{c} \sum_j X_{i,j} \right]^2} \right]^2 \quad (4)$$

2.4 Estimating Cardiac and Respiratory Phase

Before we can make use of the above methods, we need an estimate of the cardiac and respiratory phase at each tracked point in the feature trajectory. It would be ideal if we could acquire this information from the anaesthetist’s monitor, but not all such monitors provide an interface through which this information can be streamed. Furthermore, monitors that do support such streaming may not be exactly in phase with the intraoperative videos. So as an alternative, we propose the following phase estimation method based on the autocorrelation of the feature trajectories.

Let $x_{f,i}$ be the i^{th} element of \mathbf{x}_f , with unknown cardiac and respiratory phases χ_i and ρ_i . We estimate the cardiac periods of all cycles relative to the

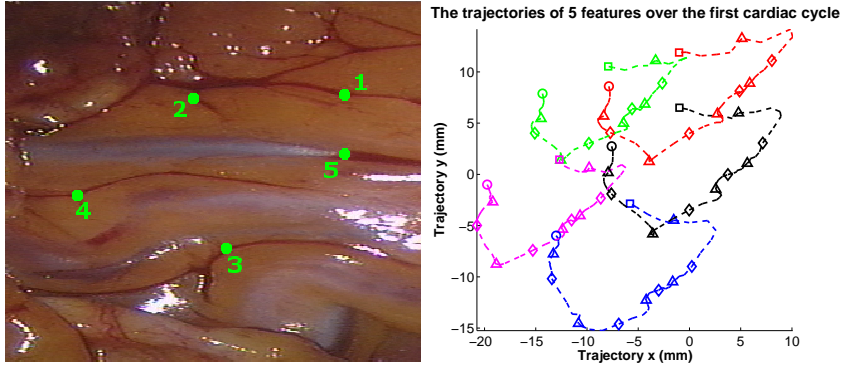


Fig. 1. (*Left*) The first frame of the video with the 5 tracked features. (*Right*) A graph of the trajectories of the 5 features over the first cardiac cycle (covering about 1 second of video). The markers indicate some corresponding frames. The circular markers are at the first frame, and the square markers at the last.

phase of $x_{f,0}$ by finding the temporal offsets λ that locally maximise the following autocorrelation function:

$$f_{\text{AUTO}}(\lambda) = \frac{1}{T - \lambda} \sum_{i=0}^{T-\lambda-1} \frac{(x_{f,i+\lambda} - \bar{x}_{f,\lambda:T-1})(x_{f,i} - \bar{x}_{f,0:T-\lambda-1})}{\sigma_{x_f,\lambda:T-1}\sigma_{x_f,0:T-\lambda-1}}, \quad (5)$$

where $\bar{x}_{f,a:b}$ and $\sigma_{x_f,a:b}$ are the mean and standard deviation of $x_{f,a}$, $x_{f,a+1}$, \dots , $x_{f,b}$.

If λ_0 and λ_1 are consecutive peaks in this function, we estimate the cardiac phase χ_t of the intermediate point $t \in [\lambda_0, \lambda_1]$ by linear interpolation:

$$\chi_t = \frac{t - \lambda_0}{\lambda_1 - \lambda_0}. \quad (6)$$

To estimate respiratory phase, we first of all filter the high frequency cardiac motion out of \mathbf{x}_f with a Gaussian convolution kernel of a suitable standard deviation (we used a standard deviation equal to a third of the mean cardiac period), and then we use the same autocorrelation method on the filtered data. Note that the precision of the phase estimates obtained by this method is limited by the frame rate of the video. To obtain higher-precision estimates, we supersampled \mathbf{x}_f using spline interpolation, before calculating f_{AUTO} .

3 Results and Discussion

We manually tracked 5 features over 1060 frames of a 50Hz video of a single patient. For given values of n_χ , n_ρ and α , we fitted the CRPM to each dimension of each feature individually, and then used 4-fold cross validation (as described

Table 1. This table summarises the RMS model fitting errors and the mean heights of the CCR error bars (see figure 2) in each dimension for the CRPMs that were fitted to the five features with parameters $n_\chi = 19$, $n_\rho = 8$ and $\alpha = 1.42$. The percentages in the ‘mean CCR error bar heights’ columns give the ratios of the mean heights of the red error bars in figure 2 to the mean heights of the green error bars. The error bounds in the ‘RMS model fitting errors’ columns are the standard deviations of the absolute errors.

Feature	Mean CCR error bar heights			RMS model fitting errors		
	x (mm)	y (mm)	z (mm)	x (mm)	y (mm)	z (mm)
1	4.91 (32%)	4.61 (35%)	11.41 (90%)	2.19±1.34	1.92±1.15	4.71±3.01
2	3.47 (26%)	2.50 (26%)	5.35 (96%)	1.38±0.91	1.05±0.66	1.89±1.12
3	3.72 (26%)	2.89 (28%)	4.13 (93%)	1.49±0.96	1.10±0.66	1.49±0.95
4	3.46 (25%)	2.48 (28%)	3.68 (83%)	1.45±0.97	1.00±0.62	1.40±0.90
5	4.39 (28%)	3.31 (28%)	9.65 (90%)	1.88±1.14	1.38±0.83	3.78±2.38
Mean:	3.99 (27%)	3.16 (30%)	6.84 (90%)	1.71±1.10	1.34±0.86	2.97±2.15

in section 2.2) to calculate an average value for $e(n_\chi, n_\rho, \alpha)$ over all dimensions and features. We searched for values of e ’s parameters that would locally-optimise this average with a hill climbing strategy over the domain $(n_\chi, n_\rho, \alpha) \in \{5, \dots, 20\} \times \{5, \dots, 20\} \times \{0, 0.01, 0.02, \dots, 2\}$. The values we found are given in the table and figures.

In table 1, the mean CCR error bar heights and RMS fitting errors in the z dimension are almost twice the errors in the x and y dimensions. This is to be expected, as the stereo endoscopic images we worked with have a very narrow baseline, and so the features would need to have been matched very accurately to attain accurate depth estimation. A good stereo matching algorithm with subpixel accuracy could potentially improve the depth estimation.

The table also shows that the errors for features 1 and 5 are significantly worse than the errors for the other 3 features. The locations of these two features were often obscured by motion blur and specular reflections, hence the errors are due to inaccurate tracking and matching.

The RMS errors for the x and y dimensions of features 2 to 4 range between 1 ± 0.62 mm and 1.49 ± 0.96 mm. These are of the same order of magnitude as the noise we expect to be introduced by tracking and matching inaccuracies. This suggests that the CRPM’s estimate of what the compound cardio-respiratory motion would look like in the absence of noise may be adequate for it to be used for further analysis of that motion in these dimensions.

Table 1 shows us that the spatial ranges of the middle 90% of the temporally-registered cardiac cycles of features 2 to 4 are still quite large (≥ 2.48 mm) after subtracting the CRPM’s respiratory component (compare these ranges to the ~ 20 mm range of total motion shown in the left column of figure 2). These errors should be reduced before using the model to analyse the cardiac and respiratory motion components individually. One possible way to reduce them may be to

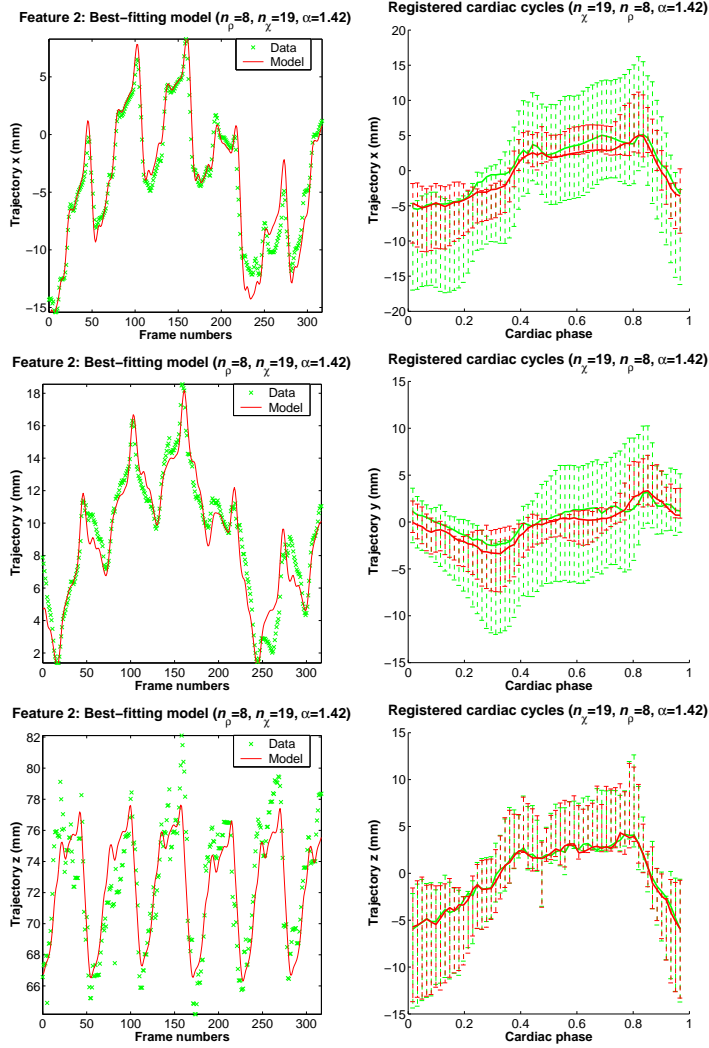


Fig. 2. (Left column) These graphs show the fit of the CRPM to the x , y and z trajectories of feature 2. (Right column) The red graphs show the spatial variations of feature 2's cardiac cycles after subtracting the CRPM's respiratory component and temporally registering them. The green graphs show the feature's temporally registered cardiac cycles before the respiratory component was subtracted, for comparison. The thick central lines denote the median trajectories, and the error bars show 45% of the data either side of the median. The ratio of the mean height of the red error bars to the mean height of the green bars gives a measure of how much subtracting the CRPM's respiratory component reduces the cardiac cycle variations. Minimising ϵ^{CCR} will minimise this ratio and vice versa. The fact that this ratio is so high in the z dimension shows that the CRPM is fitting the z noise rather than accurately estimating the respiratory and cardiac motion.

add a term to equation (2) for the CCR error, and to reformulate equation (3) to minimise this error in addition to the fitting error and respiratory curvature.

4 Future Work

It is infeasible for us to manually track enough features over multiple patients to be able to do a more comprehensive analysis at this stage. However, it is feasible for us to manually track a few features over a few cardiac cycles (one cycle is typically approximately 50 frames long). So the next step is for us to use short, manually-defined trajectories as prior information with which to parameterise the prior model of a rudimentary tracking algorithm. This should allow us to track salient features individually.

Once we have sufficient data for these salient features, we will validate alternative cardio-respiratory motion decomposition methods. Accurate motion decomposition will allow us to develop better models of the motion of individual features.

We will also evaluate models of the local, relative cardiac/respiratory motion of features. A good model of local, relative feature motion will allow us to track highly deforming regions and to improve tracking robustness by tracking salient features that are close to each other as a group. It will also provide prior information that we can use to infer the motion of features that lie in homogeneous regions near salient features. These new models will thus allow us to densely track patches on the myocardial surface. These patches can then be combined to form a reconstruction of the visible surface.

To fully realise our myocardial reconstruction goals, the final task will be to solve the problem of automatically parameterising the prior models, so as to obviate the need to do any manual tracking for new videos.

5 Conclusion

We've shown how to estimate the cardiac and respiratory phases from intra-operative videos, and we've introduced a method for validating the results of any algorithm that decomposes cardio-respiratory motions. Furthermore, we've shown that the CRPM models the compound cardio-respiratory motion of our data set with adequate accuracy, but that its estimate of the respiratory motion needs to be improved. A larger-scale study based on automatically-tracked features is needed before more general conclusions can be made.

References

1. Falk, V., Diegeler, A., Walther, T., Banusch, J., Brucerius, J., Raumans, J., Autschbach, R., Mohr, F.W.: Total endoscopic computer enhanced coronary artery bypass grafting. *European Journals of Cardio-Thoracic Surgery* **17** (2000) 38–45

2. Kappert, U., Cichon, R., Schneider, J., Gulielmos, V., Ahmadzade, T., Nicolai, J., Tugtekin, S.M., Schueler, S.: Technique of closed chest coronary artery surgery on the beating heart. *European Journals of Cardio-Thoracic Surgery* **20** (2001) 765–769
3. Dogan, S., Aybek, T., Andressen, E., Byhahn, C., Mierdl, S., Westphal, K., Matheis, G., Moritz, A., Wimmer-Greinecker, G.: Totally endoscopic coronary artery bypass grafting on cardiopulmonary bypass with robotically enhanced telemanipulation: Report of forty-five cases. *Journals of Thoracic Cardiovascular Surgery* **123** (2002) 1125–1131
4. Adhami, L., Coste-Maniere, E.: A versatile system for computer integrated mini-invasive robotic surgery. *Lecture Notes in Computer Science* **2488** (2002) 272–281
5. Szpala, S., Wierzbicki, M., Guiraudon, G., Peters, T.M.: Real-time fusion of endoscopic views with dynamic 3-d cardiac images: A phantom study. *IEEE Transactions on Medical Imaging* **24** (2005) 1207–1215
6. Falk, V., Mourgues, F., Adhami, L., Jacobs, S., Thiele, H., Nitzsche, S., Mohr, F.W., Coste-Maniere, T.: Cardio navigation: Planning, simulation, and augmented reality in robotic assisted endoscopic bypass grafting. *Annals of Thoracic Surgery* **79** (2005) 2040–2048
7. Leven, J., Burschka, D., Kumar, R., Zhang, G., Blumenkranz, S., Dai, X.T., Awad, M., Hager, G.D., Marohn, M., Choti, M., Hasser, C., Taylor, R.H.: Davinci canvas: a telerobotic surgical system with integrated, robot-assisted, laparoscopic ultrasound capability. *Lecture Notes in Computer Science* **3749** (2005) 811–818
8. Stoyanov, D., Mylonas, G.P., Deligianni, F., Darzi, A., Yang, G.Z.: Soft-tissue motion tracking and structure estimation for robotic assisted MIS procedures. *Medical Image Computing And Computer-Assisted Intervention - MICCAI 2005, Pt 2* **3750** (2005) 139–146
9. Stoyanov, D., Darzi, A., Yang, G.Z.: Dense 3d depth recovery for soft tissue deformation during robotically assisted laparoscopic surgery. In: *Medical Image Computing and Computer Assisted Interventions (MICCAI04)*. Volume 2. (2004) 48–55
10. Ortmaier, T., Groger, M., Boehm, D.H., Falk, V., Hirzinger, G.: Motion estimation in beating heart surgery. *IEEE Transactions on Biomedical Engineering* **52**(10) (October 2005) 1729–1740
11. Shechter, G., Ozturk, C., Resar, J.R., McVeigh, E.R.: Respiratory motion of the heart from free breathing coronary angiograms. *IEEE Transactions on Medical Imaging* **23**(8) (August 2004) 1046–1056